Hyperspectral Image Restoration Based on Spatio-Spectral Structure Tensor Regularization

Ryuji Kurihara
Univ. of Kitakyushu

Shunsuke Ono
Tokyo Institute of Tech.

Keiichiro Shirai
Shinshu Univ.

Masahiro Okuda
Univ. of Kitakyushu

***Abstract*—We propose a regularization function for hyperspectral image restoration based on a newly-designed structure tensor. We adopt a convex optimization approach with the use of the nuclear norm of a matrix, termed as** *spatio-spectral structure tensor*. **It consists of the gradient components of a hyperspectral image cube w.r.t. the spatio-spectral domain. The proposed approach allows to penalize variations in the spectral domain as well as the spatial domain to exploit the spatio-spectral correlations. Our experiments on denoising of hyperspectral images show that the proposed regularization leads to significant improvements in restoration performance over state-of-the-art methods.**

I. Introduction

In recent years, image processing for hyperspectral images with a large number of spectral bands has become an important issue due to the development of remote sensing and imaging technologies [1], [2]. Since a hyperspectral sensor generally acquires spectral components covering narrow spectral bands, the illuminance captured by the sensor becomes low, so noise signals are amplified together with the luminance.

To extract signals buried in the noise, many denoising methods for the hyperspectral images have been proposed [3]–[8]. BM4D [3] is a highly accurate non-local method for images with three or more channels, which is an extended version of the state-of-the-art 2D image denoising method [9]. Another effective approach is regularization based on total variation-type functions exploiting variations in the spatial domain [5]–[7], which are stated as convex optimization problems and efficiently solved to estimate a noiseless latent image.

Low-rank-based regularization approaches have also been actively investigated [10]–[14]. In [13], the correlation of the spatial structure in a local region of a multi/hyperspectral image is exploited by using structure tensor total variation (STV), and high-performance restoration can be achieved without computationally inefficient non-local search. This is because STV is defined as the nuclear norm of the structure tensor, a matrix consisting of gradient components in a local region, and thus it can evaluate the semi-local spatial correlation of images. However, STV does not measure the correlation between bands because it deals with gradient components for each band independently. To address this issue, its arranged version (ASTV) [14] has been proposed. ASTV simultaneously measures correlations between bands as well as spatial correlations, but it consists only of gradient components in spatial directions and does not explicitly exploit smoothness in the spectral direction.

In this paper, we propose a regularization function based on the structure tensor consisting of the gradient components both in the spectral domain in addition to the spatial domains. The regularization functions is then defined as the nuclear norm of the said structure tensor, so that our regularization can effectively promote the semi-local smoothness both in the spatial and spectral directions. Then, we formulate hyperspectral image restoration as a convex optimization problem involving our regularization function, which is efficiently solved by a primal-dual splitting method [15]–[17]. We apply our regularization to hyperspectral image denoising and demonstrate that it outperforms several state-of-the-art methods, namely, ASTV and BM4D.

II. Proposed Method

A. Spatio-spectral gradient filter

A hyperspectral image with M bands is denoted as $\mathbf{u} = [\mathbf{u}'^{\top}_1, \ldots, \mathbf{u}'^{\top}_M]^{\top} \in \mathbb{R}^{MN}$ (N is the number of pixels), where $\mathbf{u}'_j \in \mathbb{R}^N$ ($j = 1, \ldots, M$) is the j-th band image. The gradient filters w.r.t. the vertical and horizontal directions in a single band $\mathbf{u}'_j$ are defined as $\mathbf{D}'_v$ and $\mathbf{D}'_h \in \mathbb{R}^{N\times N}$, respectively. The matrices are extended to apply $\mathbf{D}'_v$ and $\mathbf{D}'_h$ to $\mathbf{u}$, which are defined as $\mathbf{D}_v = \mathrm{diag}(\mathbf{D}'_v, \ldots, \mathbf{D}'_v) \in \mathbb{R}^{MN\times MN}$ and $\mathbf{D}_h = \mathrm{diag}(\mathbf{D}'_h, \ldots, \mathbf{D}'_h) \in \mathbb{R}^{MN\times MN}$, respectively. The matrix $\mathbf{D}_s \in \mathbb{R}^{MN\times MN}$ for derivation w.r.t. the spectral direction is defined as follows:

$$\mathbf{D}_s = \begin{bmatrix} -\mathbf{I} & \mathbf{I} & \mathbf{O} & \cdots & \cdots & \mathbf{O} \\ \mathbf{O} & -\mathbf{I} & \mathbf{I} & \mathbf{O} & \cdots & \mathbf{O} \\ \vdots & \ddots & \ddots & \ddots & & \vdots \\ \vdots & & \mathbf{O} & -\mathbf{I} & \mathbf{I} & \mathbf{O} \\ \vdots & & & \ddots & -\mathbf{I} & \mathbf{I} \\ \mathbf{O} & \cdots & \cdots & \cdots & \mathbf{O} & \mathbf{O} \end{bmatrix},$$

ISBN 978-0-9928626-7-1

where $\mathbf{I} \in \mathbb{R}^{N\times N}$ is an identity matrix and $\mathbf{O} \in \mathbb{R}^{N\times N}$ is a zero matrix. Using $\mathbf{D}_v$, $\mathbf{D}_h$, and $\mathbf{D}_s$, a *spatio-spectral* gradient filter matrix is defined as

$$\mathbf{D} = [\mathbf{D}_v^\top \ \mathbf{D}_h^\top \ \mathbf{D}_s^\top]^\top.$$

B. Spatio-spectral structure tensor

For a given hyperspectral image $\mathbf{u}$, the gradient image is represented as $\mathbf{Du} \in \mathbb{R}^{3MN}$, and constructed by two spatial gradient images, $\mathbf{D}_v\mathbf{u}$ and $\mathbf{D}_h\mathbf{u} \in \mathbb{R}^{MN}$, and the spectral gradient image, $\mathbf{D}_s\mathbf{u} \in \mathbb{R}^{MN}$ as follows:

$$\begin{aligned}
\mathbf{Du} &= [(\mathbf{D}_v\mathbf{u})^\top \ (\mathbf{D}_h\mathbf{u})^\top \ (\mathbf{D}_s\mathbf{u})^\top]^\top, \\
\mathbf{D}_v\mathbf{u} &= [(\mathbf{D}'_v\mathbf{u}'_1)^\top \ (\mathbf{D}'_v\mathbf{u}'_2)^\top \ \dots (\mathbf{D}'_v\mathbf{u}'_M)^\top]^\top, \\
\mathbf{D}_h\mathbf{u} &= [(\mathbf{D}'_h\mathbf{u}'_1)^\top \ (\mathbf{D}'_h\mathbf{u}'_2)^\top \ \dots (\mathbf{D}'_h\mathbf{u}'_M)^\top]^\top, \\
\mathbf{D}_s\mathbf{u} &= [(\mathbf{D}'_s\mathbf{u}'_1)^\top \ (\mathbf{D}'_s\mathbf{u}'_2)^\top \ \dots (\mathbf{D}'_s\mathbf{u}'_M)^\top]^\top.
\end{aligned} \quad (1)$$

We divide the gradient images into 3D local blocks. The shape of each local block is a rectangular block with a square base in the spatial domain, and each block contains all the bands (e.g. the size of the block is $10 \times 10 \times M$). The arrangement of the matrix is illustrated in Fig.1. We define a new structure tensor of the n-th local block by rearranging the matrices as follows:

$$\mathbf{L}_n = [\mathbf{Du}_1^{(n)} \ \mathbf{Du}_2^{(n)} \ \dots \mathbf{Du}_M^{(n)}] \in \mathbb{R}^{N'\times 3M}, \quad (2)$$

where N' is the number of pixels in a single band of a local block. $\mathbf{Du}_j^{(n)} = [\mathbf{D}_v\mathbf{u}_j^{(n)} \ \mathbf{D}_h\mathbf{u}_j^{(n)} \ \mathbf{D}_s\mathbf{u}_j^{(n)}] \in \mathbb{R}^{N'\times 3}$ $(j = 1, \dots, M)$, and $\mathbf{D}_*\mathbf{u}_j^{(n)}$ consists of the j-th band in the n-th local block. We call $\mathbf{L}_n$ in (2) a *spatio-spectral structure tensor*. In the next section, we construct a convex optimization problem with a regularization function based on the spatio-spectral structure tensor to restore a latent hyperspectral image.

C. Regularization based on spatio-spectral structure tensor

In the paper, we focus on hyperspectral image denoising as an example of hyperspectral image restoration. We remark that our regularization can be applied to other problems such as non-blind image deblurring and compressive sensing.

We assume that the degradation process can be modeled as $\mathbf{y} = \mathbf{u} + \mathbf{n}$, where $\mathbf{y} \in \mathbb{R}^{MN}$ is an observation image and $\mathbf{n} \in \mathbb{R}^{MN}$ is the additive white Gaussian noise. Regularization based on the aforementioned spatio-spectral structure tensor can be defined as the sum of rank$(\mathbf{L}_n)$ $(n = 1, 2, \cdots, K)$ with two constraints. One is a constraint on the intensity range $\mathcal{S} = [0, 1]^{MN}$. The other constraint represents data-fidelity, defined by the $\mathbf{y}$-centered L2-norm ball with the radius $\epsilon > 0$ controlling the degree of fidelity to $\mathbf{y}$. Compared with

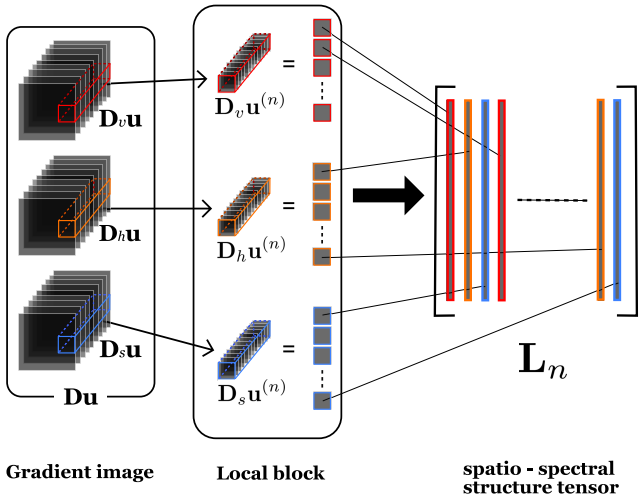

Fig. 1. Spatio-spectral structure tensor

the standard additive data-fidelity, such a constraint-type data-fidelity facilitates parameter setting because ϵ has a clear physical meaning, so that it can be easily adjusted based on noise standard deviation, as addressed in [18]–[21]. Specifically we consider the following optimization problem:

$$\min_{\mathbf{x}} \sum_{n=1}^{K} \mathrm{rank}(\mathbf{L}_n) \quad s.t. \ \mathbf{x} \in \mathcal{S}, \ \|\mathbf{x}-\mathbf{y}\|_2 \le \epsilon, \quad (3)$$

where K is the number of extracted local blocks, and all pixels of $\mathbf{x}$ are extracted at least once as a pixel of a local block. Here, $\mathbf{L}_n$ is represented with an operator $\mathbf{P}_n : \mathbb{R}^{3MN} \to \mathbb{R}^{3MN'}$ that extracts the n-th local block as

$$\mathbf{L}_n = \mathbf{P}_n\mathbf{Dx}. \quad (4)$$

Substituting this for Eq.(3) yields

$$\min_{\mathbf{x}} \sum_{n=1}^{K} \mathrm{rank}(\mathbf{P}_n\mathbf{Dx}) \quad s.t. \ \mathbf{x} \in \mathcal{S}, \ \|\mathbf{x}-\mathbf{y}\|_2 \le \epsilon. \quad (5)$$

Since rank$(\cdot)$ is the nonconvex function that counts the number of non-zero singular values, which makes it intractable to find the optimal solution, we introduce the nuclear norm $\|\cdot\|_* = \sum_i \sigma_i$ (σ_i is the singular values) [22], which is a reasonable convex relaxation for rank$(\cdot)$. Thus the problem (5) is converted to the following convex optimization problem:

$$\min_{\mathbf{x}} \sum_{n=1}^{K} \|\mathbf{P}_n\mathbf{Dx}\|_* \quad s.t. \ \mathbf{x} \in \mathcal{S}, \ \|\mathbf{x}-\mathbf{y}\|_2 \le \epsilon. \quad (6)$$

ISBN 978-0-9928626-7-1 © EURASIP 2017

We further reformulate (6) into the following form:

$$\min_{\mathbf{x}} \sum_{n=1}^{K} \|\mathbf{P}_n \mathbf{D}\mathbf{x}\|_* + \iota_{\mathcal{S}}(\mathbf{x}) + \iota_{\mathcal{B}_{\mathbf{y},\epsilon}}(\mathbf{x}), \tag{7}$$

where $\mathcal{S}$ is the closed convex set used in (3), and the indicator function is defined as

$$\iota_{\mathcal{S}}(\mathbf{x}) = \begin{cases} 0 & \mathbf{x} \in \mathcal{S}, \\ +\infty & \text{otherwise.} \end{cases} \tag{8}$$

The set $\mathcal{B}_{\mathbf{y},\epsilon}$ is defined as $\mathcal{B}_{\mathbf{y},\epsilon} = \{\mathbf{x} \in \mathbb{R}^{MN} \mid \|\mathbf{x} - \mathbf{y}\|_2 \leq \epsilon\}$ using the prescribed error tolerance ϵ, and $\iota_{\mathcal{B}_{\mathbf{y},\epsilon}}(\mathbf{x})$ is defined in the same way as (8).

D. Optimization

For solving the convex optimization problem in (7), we use a *primal-dual splitting* (PDS) method [15]–[17]. The PDS handles convex optimization problems of the form:

$$\min_{\mathbf{x}} F(\mathbf{x}) + G(\mathbf{x}) + H(\mathbf{A}\mathbf{x}), \tag{9}$$

where F is a differentiable convex function whose gradient is β-Lipschitz continuous, G and H are possibly nonsmooth convex functions whose proximity operators [1] are computable, and $\mathbf{A}$ is a linear operator. The algorithm for (9) is given by

$$\begin{cases} \mathbf{x}^{(k+1)} = \mathrm{prox}_{\gamma_1 G}(\, \mathbf{x}^{(k)} - \gamma_1(\nabla F(\mathbf{x}^{(k)}) + \mathbf{A}^\top \mathbf{z}^{(k)})\,), \\ \mathbf{z}^{(k+1)} = \mathrm{prox}_{\gamma_2 H^*}(\, \mathbf{z}^{(k)} + \gamma_2 \mathbf{A}(2\mathbf{x}^{(\mathbf{k+1})} - \mathbf{x}^{(\mathbf{k})})\,), \end{cases} \tag{10}$$

where ∇F is the gradient of F, $\mathbf{A}^\top$ is the transpose of $\mathbf{A}$, $\mathbf{x}$ is the primal variable and $\mathbf{z}$ is the dual variable. H^* is the conjugate function of H, and its proximity operator can be computed using the proximity operator of H, given by

$$\mathrm{prox}_{\gamma_2 H^*}(\mathbf{v}) = \mathbf{v} - \gamma_2 \mathrm{prox}_{\gamma_2^{-1} H}(\gamma_2^{-1}\mathbf{v}). \tag{11}$$

Under appropriate conditions on γ_1 and γ_2, the sequence generated by (10) converges to an optimal solution of (9). In order to apply PDS to our problem (7), we define F, G, H, and $\mathbf{A}$ as follows

$$\begin{aligned} F &: \mathbb{R}^{MN} \to \mathbb{R}, \quad \mathbf{x} \mapsto 0, \\ G &: \mathbb{R}^{MN} \to \mathbb{R} \cup \{\infty\}, \quad \mathbf{x} \mapsto \iota_{\mathcal{S}}(\mathbf{x}), \\ H &: \mathbb{R}^{MN'+MN} \to \mathbb{R} \cup \{\infty\}, \\ &\quad \mathbf{z} = [\mathbf{z}_1^\top, \mathbf{z}_2^\top]^\top \mapsto \sum_{n=1}^{K} \|\mathbf{z}_{1,n}\|_* + \iota_{\mathcal{B}_{\mathbf{y},\epsilon}}(\mathbf{z}_2), \\ \mathbf{A} &: \mathbb{R}^{MN} \to \mathbb{R}^{3MN'+MN}, \quad \mathbf{x} \mapsto (\mathbf{P}_n \mathbf{D}\mathbf{x}, \mathbf{x}), \end{aligned}$$

[1]The proximity operator (prox) [23], [24] is defined as $\mathrm{prox}_{\gamma H}(\mathbf{x}) = \arg\min_{\mathbf{a}} H(\mathbf{a}) + \frac{1}{2\gamma}\|\mathbf{a} - \mathbf{x}\|_2^2$.

Algorithm 1 Algorithm for solving Prob. (7)

1: input : $\mathbf{x}^{(0)}$, $\mathbf{z}_{1,n}^{(0)} (n = 1, ..., K)$, $\mathbf{z}_2^{(0)}$
2: set : γ_1, and γ_2 are given.
3: **while** stopping criterion is satisfied. **do**
4: $\quad \mathbf{x}^{(k+1)} = P_{\mathcal{S}}(\mathbf{x}^{(k)} - \gamma_1(\sum_{n=1}^{K} \mathbf{D}^\top \mathbf{P}_n^\top \mathbf{z}_{1,n}^{(k)} + \mathbf{z}_2^{(k)}))$
5: $\quad$ **for** $n = 1$ to K **do**
6: $\quad\quad \mathbf{v}_{1,n}^{(k)} = \mathbf{z}_{1,n}^{(k)} + \gamma_2(\mathbf{P}_n \mathbf{D}(2\mathbf{x}^{(k+1)} - \mathbf{x}^{(k)}))$
7: $\quad\quad \mathbf{z}_{1,n}^{(k+1)} = \mathbf{v}_{1,n}^{(k)} - \gamma_2 \mathrm{prox}_{\frac{1}{\gamma_2}\|\cdot\|_*}(\frac{1}{\gamma_2}\mathbf{v}_{1,n}^{(k)})$
8: $\quad$ **end for**
9: $\quad \mathbf{v}_2^{(k)} = \mathbf{z}_2^{(k)} + \gamma_2(2\mathbf{x}^{(k+1)} - \mathbf{x}^{(k)})$
10: $\quad \mathbf{z}_2^{(k+1)} = \mathbf{v}_2^{(k)} - \gamma_2 \mathrm{prox}_{\frac{1}{\gamma_2}\iota_{\mathcal{B}_{\mathbf{y},\epsilon}}}(\frac{1}{\gamma_2}\mathbf{v}_2^{(k)})$
11: $\quad k = k + 1$
12: **end while**

where $\mathbf{z}_{1,n}$ represents the n-th local block of $\mathbf{z}_1$. The steps of the algorithm for solving (7) are shown in Algorithm 1, where $P_{\mathcal{S}}$ in the 4th line is projection onto the convex set $\mathcal{S}$, which transfers pixel values within the range. The proximity operator of the nuclear norm in the 7th line is obtained by applying singular value decomposition to $\mathbf{L}_n$ and then thresholding the singular values:

$$\begin{aligned} &\mathrm{prox}_{\gamma\|\cdot\|_*}(\mathbf{L}_n) = \mathbf{U}\tilde{\Sigma}\mathbf{V}^\top, \\ &\tilde{\Sigma} = \mathrm{diag}(\max\{\sigma_1 - \gamma, 0\}, \ldots, \max\{\sigma_{3M} - \gamma, 0\}). \end{aligned} \tag{12}$$

The proximity operator of the indicator function $\iota_{\mathcal{B}_{\mathbf{y},\epsilon}}$ is given by the convex projection onto the l_2 ball (10th line):

$$\mathrm{prox}_{\gamma\iota_{\mathcal{B}_{\mathbf{y},\epsilon}}}(\mathbf{x}) = \begin{cases} \mathbf{x} & \mathbf{x} \in \mathcal{B}_{\mathbf{y},\epsilon}, \\ \mathbf{y} + \frac{\epsilon}{\|\mathbf{x}-\mathbf{y}\|_2}(\mathbf{x} - \mathbf{y}) & \text{otherwise.} \end{cases} \tag{13}$$

III. EXPERIMENTAL RESULTS

In order to evaluate the performance of the proposed method, we compare it with ASTV [14] and BM4D [3] on denoising of hyperspectral images. We assume that input images are degraded by additive white Gaussian noise $\mathbf{n} \in \mathbb{R}^{MN}$ with standard deviation of 0.1. The parameter ϵ in (6) is appropriately changed depending on the noise intensity. All pixel values are normalized to within the range $[0, 1]$. The size of the local blocks (in the block processing of the nuclear norm in both of the methods) was set to $10 \times 10 \times M$, and there is no overlap between them[2]. As for BM4D, we use the

[2]On the basis of our experience, the block overlap significantly increases computational complexity, while we achieve it with only a little improvement in restoration performance.

ISBN 978-0-9928626-7-1 © EURASIP 2017

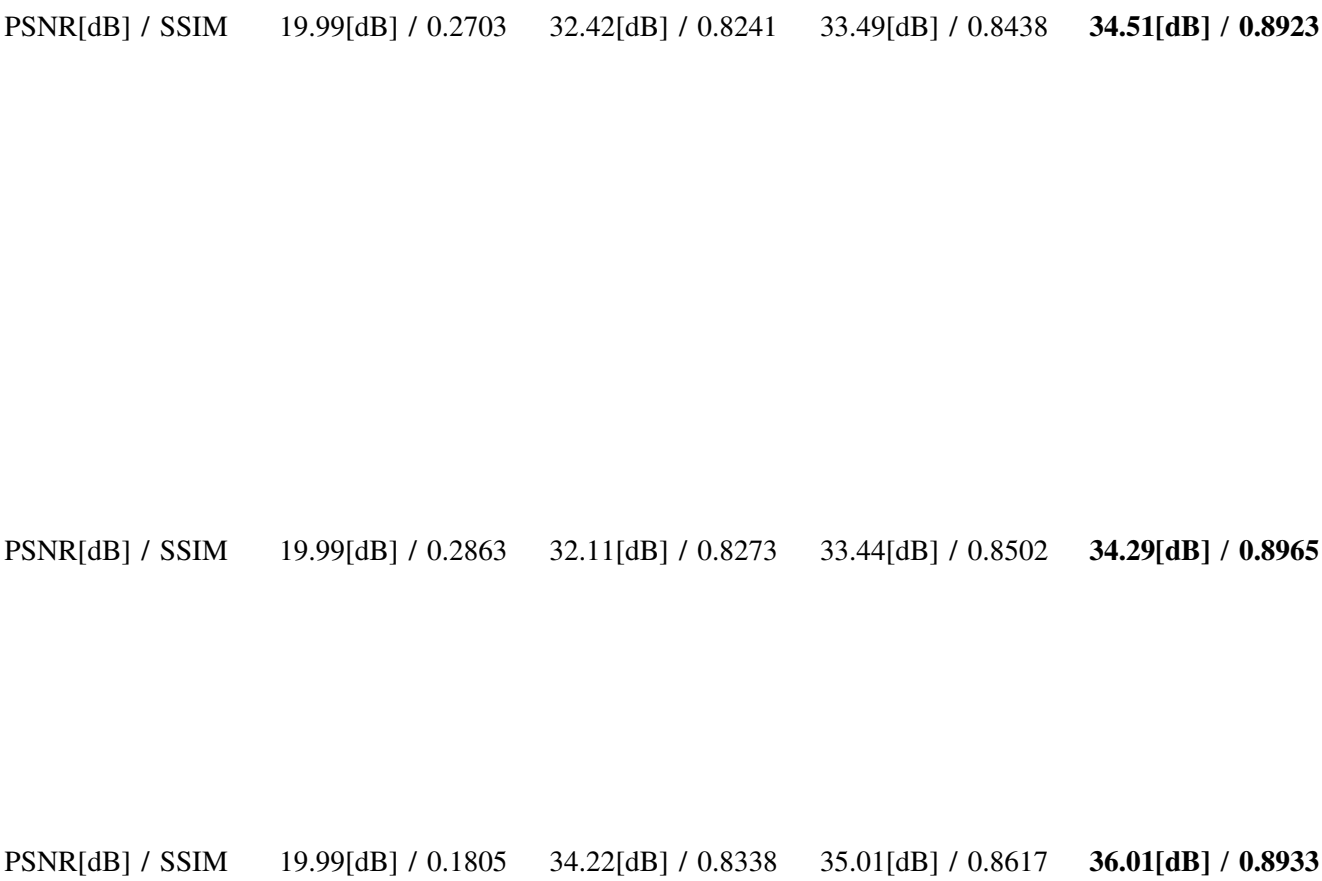

Fig. 2. Results in PaviaC (102 bands) (upper), PaviaU (103 bands) (middle) and Frisco(148 bands) (lower) : from left, Original, Noisy, ASTV [14], BM4D [3], and ours

MATLAB code published by the authors. Test images were taken from the images in [8], [25], [26]. In order to objectively evaluate denoising performance, two indexes: peak signal to noise ratio (PSNR) and SSIM [27] are used.

The quantitative evaluation of denoising performance by PSNR and SSIM is shown in Tables I and II, respectively. The experimental results for three hyperspectral images, PaviaC (102 bands), PaviaU (103 bands), and Frisco (148 bands) are shown in Fig.2, in which we show the 95th band in the PaviaC, the 98th band in the PaviaU and the 130th band in the Frisco. It can be seen from Fig.2 that the proposed method can achieve satisfactory denoising performance while maintaining details compared to the conventional methods. In quantitative evaluations in Tables I and II, it can be confirmed that the quantitative performance of noise removal in the proposed method outperforms the conventional ones.

IV. CONCLUSION

In this paper, we proposed a regularization method based on the spatio-spectral structure tensor aiming at restoration of hyperspectral images. The proposed method simultaneously exploits two properties. One is

ISBN 978-0-9928626-7-1 © EURASIP 2017

TABLE I
COMPARISON WITH [14] AND [3] (IN PSNR[DB])

Image	(bands)	ASTV [14]	BM4D [3]	Ours
China	(7)	**32.51**	32.02	32.05
Ribeira	(33)	34.49	34.62	**35.84**
PaviaC	(102)	32.42	33.49	**34.51**
PaviaU	(103)	32.11	33.44	**34.29**
Frisco	(148)	34.22	35.01	**36.01**
Stanford	(148)	34.45	35.31	**36.34**
Salinas	(224)	35.03	**36.76**	36.50

TABLE II
COMPARISON WITH [14] AND [3] (IN SSIM)

Image	(bands)	ASTV [14]	BM4D [3]	Ours
China	(7)	**0.8729**	0.8534	0.8521
Ribeira	(33)	0.8652	0.8740	**0.9077**
PaviaC	(102)	0.8241	0.8438	**0.8923**
PaviaU	(103)	0.8273	0.8502	**0.8965**
Frisco	(148)	0.8338	0.8617	**0.8933**
Stanford	(148)	0.8229	0.8649	**0.8846**
Salinas	(224)	0.8106	**0.8720**	0.8625

the low-rank property of gradient images w.r.t. the spatio-spectral directions in the hyperspectral image, and the other is the correlation between spectral bands. By solving the convex optimization problem using some regularization, high performance method in denoising for hyperspectral images is achieved. The experimental results demonstrate that the proposed method outperforms the conventional methods.

REFERENCES

[1] J.M. Bioucas-Dias, A. Plaza, G. Camps-Valls, P. Scheunders, N. Nasrababi, and J. Chanussot, "Hyperspectral remote sens. data analysis and future challenges," *IEEE Geosci. Remote Sens. Magazine*, vol. 1, no. 2, pp. 6–36, 2013.

[2] G. Shaw and D. Manolakis, "Signal processing for hyperspectral image exploitation," *IEEE Signal Process. Magazine*, vol. 19, no. 1, pp. 12–16, 2002.

[3] M. Maggioni, V. Katkovnik, K. Egiazarian, and A. Foi, "Nonlocal transform-domain filter for volumetric data denoising and reconstruction," *IEEE T. Image Process.*, vol. 22, no. 1, pp. 119–133, 2013.

[4] J. Atkinson, F. Kamalabadi, and D. L Jones, "Wavelet-based hyperspectral image estimation," in *Proc. IEEE Int. Geosci. Remote Sens. Symp.*, 2003, vol. 2, pp. 743–745.

[5] Q. Yuan, L. Zhang, and H. Shen, "Hyperspectral image denoising employing a spectral–spatial adaptive total variation model," *IEEE T. Geosci. Remote Sens.*, vol. 50, no. 10, pp. 3660–3677, 2012.

[6] H.K. Aggarwal and A. Majumdar, "Hyperspectral image denoising using spatio-spectral total variation," *IEEE Geosci. Remote Sens. Lett.*, vol. 13, no. 3, pp. 442–446, 2016.

[7] S. Takeyama, S. Ono, and I. Kumazawa, "Hyperspectral image restoration by hybrid spatio-spectral total variation," in *Proc. IEEE Int. Conf. Acoust. Speech Signal Process.*, 2017.

[8] M. Rizkinia, T. Baba, K. Shirai, and M. Okuda, "Local spectral component decomposition for multi-channel image denoising," *IEEE T. Image Process.*, vol. 25, no. 7, pp. 3208–3218, 2016.

[9] K. Dabov, A. Foi, V. Katkovnik, and K. Egiazarian, "Image denoising by sparse 3-d transform-domain collaborative filtering," *IEEE T. Image Process.*, vol. 16, no. 8, pp. 2080–2095, 2007.

[10] Y.Q. Zhao and J. Yang, "Hyperspectral image denoising via sparse representation and low-rank constraint," *IEEE T. Geosci. Remote Sens.*, vol. 53, no. 1, pp. 296–308, 2015.

[11] H. Zhang, W. He, L. Zhang, H. Shen, and Q. Yuan, "Hyperspectral image restoration using low-rank matrix recovery," *IEEE T. Geosci. Remote Sens.*, vol. 52, no. 8, pp. 4729–4743, 2014.

[12] B. Rasti, J.R Sveinsson, and M.O. Ulfarsson, "Wavelet-based sparse reduced-rank regression for hyperspectral image restoration," *IEEE T. Geosci. Remote Sens.*, vol. 52, no. 10, pp. 6688–6698, 2014.

[13] S. Lefkimmiatis, A. Roussos, P. Maragos, and M. Unser, "Structure tensor total variation," *SIAM J. Imag. Sci.*, vol. 8, no. 2, pp. 1090–1122, 2015.

[14] S. Ono, K. Shirai, and M. Okuda, "Vectorial total variation based on arranged structure tensor for multichannel image restoration," in *Proc. IEEE Int. Conf. Acoust. Speech Signal Process.*, 2016, pp. 4528–4532.

[15] L. Condat, "A primal-dual splitting method for convex optimization involving Lipschitzian, proximable and linear composite terms," *J. Optim. Theory Appl.*, vol. 158, no. 2, pp. 460–479, 2013.

[16] A. Chambolle and T. Pock, "A first-order primal-dual algorithm for convex problems with applications to imaging," *J. Math. Imag. Vis.*, vol. 40, no. 1, pp. 120–145, 2010.

[17] P. L Combettes and J.C. Pesquet, "Primal-dual splitting algorithm for solving inclusions with mixtures of composite, lipschitzian, and parallel-sum type monotone operators," *Set-Valued Variation. Anal.*, vol. 20, no. 2, pp. 307–330, 2012.

[18] M.V. Afonso, J.M. Bioucas-Dias, and M. Figueiredo, "An augmented lagrangian approach to the constrained optimization formulation of imaging inverse problems," *IEEE T. Image Process.*, vol. 20, no. 3, pp. 681–695, 2011.

[19] M. Carlavan and L. Blanc-Féraud, "Sparse poisson noisy image deblurring," *IEEE T. on Image Process.*, vol. 21, no. 4, pp. 1834–1846, 2012.

[20] G. Chierchia, N. Pustelnik, J.C. Pesquet, and B. Pesquet-Popescu, "Epigraphical projection and proximal tools for solving constrained convex optimization problems," *Signal, Image Video Process.*, vol. 9, no. 8, pp. 1737–1749, 2015.

[21] S. Ono and I. Yamada, "Signal recovery with certain involved convex data-fidelity constraints," *IEEE T. Signal Process.*, vol. 63, no. 22, pp. 6149–6163, 2015.

[22] M. Fazel, *Matrix rank minimization with applications*, Ph.D. thesis, Stanford Univ., 2002.

[23] J.J. Moreau, "Fonctions convexes duales et points proximaux dans un espace hilbertien," *C.R. Acad. Sci. Paris Ser. A Math.*, vol. 255, pp. 2897–2899, 1962.

[24] P.L. Combettes and J.C. Pesquet, *Proximal splitting methods in signal processing*, Springer, 2011.

[25] M.C. Larabi and S. Süsstrunk, "Evaluation of a hyperspectral image database for demosaicking purposes," in *Proc. SPIE Electronic Imaging*. International Society for Optics and Photonics, 2011, pp. 1–12.

[26] "The stanford center for image systems engineering," https://scien.stanford.edu/.

[27] Z. Wang, A.C Bovik, H.R Sheikh, and E.P Simoncelli, "Image quality assessment: from error visibility to structural similarity," *IEEE T. Image Process.*, vol. 13, no. 4, pp. 600–612, 2004.

ISBN 978-0-9928626-7-1 © EURASIP 2017